Simulation of modern and middle Cretaceous marine $\delta^{18}O$ with an ocean-atmosphere general circulation model

J. Zhou,[1] C. J. Poulsen,[1] D. Pollard,[2] and T. S. White[2]

Received 18 January 2008; revised 16 May 2008; accepted 1 July 2008; published 30 September 2008.

[1] We have developed a coupled ocean-atmosphere general circulation model, the GENESIS-MOM model, with the ability to transport and fractionate water isotopes in the ocean and atmosphere. The model is used to predict modern and Cretaceous precipitation and seawater $\delta^{18}O$. The model reproduces the large-scale modern-day isotopic distribution. In the zonal mean, the difference between simulated and observed seawater $\delta^{18}O$ is within 0.2‰ in the low and middle latitudes and within 1‰ at high latitudes. In comparison to modern, simulated Cretaceous surface seawater $\delta^{18}O$ is systematically depleted by 0.3‰ at low and middle latitudes. These differences are attributed to equilibrium fractionation during surface evaporation at low latitudes and an increased partitioning of ^{18}O from the surface into the deep ocean due to intermediate and deep water formation in subtropical basins in the Cretaceous. We also find that regional seawater $\delta^{18}O$ is significantly influenced by the paleobathymetry and the resolution of oceanic gateways, boundary conditions that are not well known for the past. Our simulation of Cretaceous seawater $\delta^{18}O$ has major implications for oxygen isotope paleothermometry. We conclude that conventional assumptions of past seawater $\delta^{18}O$ may lead to an overestimate of Cretaceous sea-surface temperatures, especially at middle and high latitudes.

Citation: Zhou, J., C. J. Poulsen, D. Pollard, and T. S. White (2008), Simulation of modern and middle Cretaceous marine $\delta^{18}O$ with an ocean-atmosphere general circulation model, *Paleoceanography*, *23*, PA3223, doi:10.1029/2008PA001596.

1. Introduction

[2] The middle Cretaceous (Albian-Turonian) is considered one of the warmest periods in Earth history. This inference is supported by sedimentological evidence of ice-free polar regions [*Jenkyns et al.*, 2004; *Moriya et al.*, 2007; *Price*, 1999] and paleofloral and faunal evidence of tropical species at high latitudes [*Huber*, 1998; *Nathorst*, 1911; *Spicer and Parrish*, 1986; *Tarduno et al.*, 1998], and leaf margin analyses of fossil leaves [*Parrish and Spicer*, 1988; *Herman and Spicer*, 1996]. The most direct evidence for warm conditions comes from oxygen isotope paleothermometry, which provides a quantitative estimate of past seawater temperatures. Recent estimates of past seawater temperatures using oxygen isotope paleothermometry are as high as 33–39°C at low latitudes to > 14°C at high latitudes [*Huber et al.*, 1995; *Norris et al.*, 2002; *Wilson et al.*, 2002; *Bice et al.*, 2006; *Pucéat et al.*, 2007]. However, these oxygen isotope temperature estimates are dependent on assumptions about the mean isotopic composition of Cretaceous seawater.

[3] The oxygen isotope paleothermometer works because natural fractionation processes in seawater are temperature-dependent. Because of an equilibrium effect, water molecules with ^{16}O are preferentially evaporated from seawater to produce vapor. Importantly, the equilibriuim fractionation factor decreases with increasing seawater temperature, causing the seawater isotopic composition to become enriched in ^{16}O and depleted in ^{18}O. The ambient isotopic composition of past seawater is ultimately sampled and preserved through precipitation of marine carbonates, e.g., shells of foraminifera or fish teeth. Though the isotopic composition of marine carbonates ($\delta^{18}O_c$) is often offset from seawater because of biotic effects during carbonate precipitation, laboratory and field experiments have established that the relative isotopic abundance in many species is preserved [e.g., *Shackleton*, 1974; *Erez and Luz*, 1983; *Kolodny et al.*, 1983; *Bemis et al.*, 1998].

[4] In addition to $\delta^{18}O_c$, the mean isotopic composition of seawater $\delta^{18}O_w$ must be known to calculate paleotemperature. $\delta^{18}O_w$ is known for the modern and Holocene and varies regionally [*Zachos et al.*, 1994]. The $\delta^{18}O_w$ of earlier periods is not known and is an important source of uncertainty in reconstructing paleotemperature. Cretaceous paleotemperatures have conventionally been estimated using a global mean $\delta^{18}O_w$ of −1.0‰ (SMOW) reflecting the absence of continental ice sheets during this time [*Shackleton and Kennett*, 1975], even though it is highly improbable that $\delta^{18}O_w$ was uniform across the Cretaceous oceans. Using a uniform $\delta^{18}O_w$ yields paleotemperature estimates that are lower at low latitudes and higher at high latitudes than estimates made using a latitudinally varying $\delta^{18}O_w$ [*Poulsen et al.*, 1999b]. Because a uniform $\delta^{18}O_w$ was unlikely, Cretaceous paleotemperatures are frequently estimated using both global mean Cretaceous seawater and modern local $\delta^{18}O_w$ corrected by −1.0‰ [e.g., *Norris et al.*, 2002; *Wilson et al.*, 2002; *Pucéat et al.*, 2007]. However, it is not

[1]Department of Geological Sciences, University of Michigan, Ann Arbor, Michigan, USA.
[2]Earth and Environment Science Institute, Pennsylvania State University, University Park, Pennsylvania, USA.

0883-8305/08/2008PA001596

clear that using modern corrected $\delta^{18}O_w$ is justified, or an improvement over global mean $\delta^{18}O_w$.

[5] To test these assumptions, we have recently developed a coupled ocean-atmosphere general circulation model (GCM) with the capability to transport and fractionate water isotopes in the oceans and atmosphere. This model represents a significant advance over previous climate modeling studies of Cretaceous water isotopes [e.g., *Roche et al.*, 2006; *Poulsen et al.*, 2007b]. Here, we describe and discuss our simulations of modern and Cretaceous seawater and precipitation $\delta^{18}O$, and their comparison with modern measured $\delta^{18}O$. Our results show that the distribution of Cretaceous surface $\delta^{18}O_w$ is largely similar to that of the modern. Significant differences occur in the low latitudes, where Cretaceous surface $\delta^{18}O_w$ is slightly lower, and the Arctic Ocean. The physical (nonisotopic) oceanographic results of our simulations and the isotopic comparison with Cretaceous proxies will be the focus of a subsequent paper.

2. Methods

[6] The experiments presented here were developed using the GENESIS version 3.0 Earth system model coupled to the MOM2 oceanic GCM. GENESIS is composed of an atmospheric GCM coupled to multilayer models of vegetation, soil and land ice, and snow [*Thompson and Pollard*, 1997]. In comparison to GENESIS version 2.3, the solar and infrared radiation scheme has been replaced with that used in NCAR's CCM3 [*Kiehl et al.*, 1998]. Our version of GENESIS also includes water isotopic transport and fractionation in the atmospheric physics [*Mathieu et al.*, 2002]. Building on previous isotopic GCM development by *Jouzel et al.* [1994] and *Joussaume and Jouzel* [1993], the O^{18}/O^{16} and D/H ratios are predicted in atmospheric vapor, liquid, ice, and soil water reservoirs. Fractionation is modeled as a result of condensation and evaporation in the free atmosphere and from surface waters. Atmospheric ratios are transported using the same Lagrangian transport as for bulk vapor and clouds. GENESIS-MOM does not currently include a river routing scheme, and continental river runoff is globally averaged and uniformly spread over the world ocean. Such an approximation is appropriate for the Cretaceous where major river drainage basins are not known in detail, and makes the modern simulations consistent with the Cretaceous regarding runoff.

[7] We have previously used GENESIS with isotope capabilities to predict water isotopes in atmospheric vapor [*Poulsen et al.*, 2007a, 2007b]. In this study, we add the ability to calculate isotope transport through the ocean by coupling GENESIS to MOM2, a three-dimensional, z-coordinate ocean GCM with passive tracer capabilities [*Pacanowski*, 1995]. MOM2 has a horizontal grid spacing of approximately 3.75°, and 20 vertical levels. To ensure conservation of energy and mass, the horizontal grid has been adjusted with a cosine-weighted distortion in order to match the T31 spectral grid used in GENESIS. In our implementation of MOM2, we use an isopycnal mixing scheme [*Redi*, 1982]. Coefficients of horizontal viscosity and diffusion are 2×10^9 cm^2 s^{-1} and 0.5×10^7 cm^2 s^{-1}; coefficients of vertical viscosity and diffusion are 1.0 cm^2 s^{-1} and 0.2 cm^2 s^{-1}. MOM2 also includes a full convection scheme [*Marotzke*, 1991; *Rahmstorf*, 1993], which removes buoyancy instabilities within a water column. Water isotopes are advected, diffused and convectively mixed as passive tracers within the ocean.

[8] Sea-surface isotopic fluxes due to hydrological processes, including precipitation/evaporation, river runoff, and sea ice formation/melt, are calculated in GENESIS and then passed to MOM2. As documented by *Mathieu et al.* [2002], sea ice is treated as a two-layer isotopic reservoir. In the lower layer, the isotopic content of sea ice is estimated from the isotopic composition of seawater with the appropriate isotopic fractionation. The accumulation of snow on sea ice is tracked in the upper layer. Rain on sea ice is treated as runoff. Surface isotopic fluxes from continental runoff are implicitly estimated to maintain the all-ocean mean isotopic content; this treatment is fully consistent with the global runoff treatment described above.

[9] The GENESIS and MOM models can be fully coupled, exchanging heat, moisture, and momentum fluxes every 6 h. However, in order to make long integrations (>5000 years), we have developed an alternating synchronous-asynchronous coupling technique that works as follows:

[10] 1. Fully coupled synchronous segments of 35 years are run, with atmospheric-ocean exchanges performed at each OGCM time step of 6 h. During the last 10 years of each segment, monthly mean near-surface meteorology (air temperature, humidity, winds, downward solar and infrared radiative fluxes, precipitation, and the isotopic fractionation of precipitation and evaporation) were stored as 10-year averages.

[11] 2. Following each synchronous segment, the saved fluxes are then used to drive the OGCM alone through the next asynchronous segment of 500–2000 years, with ocean surface fluxes calculated by the AGCM's (LSX) boundary layer routine using the previously saved atmospheric conditions and the current OGCM sea-surface temperatures. (Sea ice is considered part of the AGCM, and where sea ice exists in the synchronous segments, all saved "surface meteorological" quantities are those at the sea ice base.)

[12] 3. A final 35 year fully coupled synchronous segment is completed to produce data for analyses. This synchronous-asynchronous scheme has already been applied to approach equilibrium in previous work [e.g., *Kim et al.*, 2003; *Voss and Sausen*, 1996].

[13] Modern and Cretaceous simulations were integrated through at least 4 asynchronous-asynchronous segments, representing integration durations of more than 6000 years. After these long integrations, the ocean is very close to equilibrium. Global average temperature trends are 0.15°C/ka and −0.05°C/ka for Cretaceous and modern experiments, respectively. In the upper ocean (top 25 m), seawater temperature trends are 0.08°C/ka and 0.01°C/ka, respectively. In addition, $\delta^{18}O$ is well conserved in all experiments. Global average ocean $\delta^{18}O$ is −1.0 and −0.0‰ (SMOW) for the Cretaceous and modern experiments, identical to the initial values of −1.0 and −0.0‰ (SMOW).

[14] Four climate-isotope experiments were completed in this study (Table 1). Two modern experiments were com-

Table 1. Model Parameters and Global Average Sea-Surface Temperature, Precipitation, and $\delta^{18}O$ of Surface Seawater and Precipitation (SMOW)[a]

Experiment	Description	pCO_2 (ppm)	SST (°C)	Precipitation (mm/d)	Precipitation $\delta^{18}O$ (‰)	Seawater $\delta^{18}O$ (‰)
MOD	modern geography and bathymetry but with no Bering Strait	355	18.4	3.0	−7.1	0
MOD-Bering	modern geography and bathymetry with Bering Strait resolved	355	18.2	3.0	−7.1	0
K-Flat	Cenomanian geography and topography; ocean bathymetry is uniformly 5600 m	2240	23.0	3.5	−6.1	−1.0
K-Bathy	Cenomanian geography and topography; ocean bathymetry is based on PALEOMAP project reconstruction[b]	2240	23.0	3.5	−6.2	−1.0

[a]The $\delta^{18}O$ of Cretaceous seawater is "uncorrected" in this table. As noted in section 2 and the captions of Figures 5–9, a "corrected" Cretaceous $\delta^{18}O$ is generally used throughout this manuscript to facilitate comparisons between modern and Cretaceous $\delta^{18}O$. The "corrected" Cretaceous $\delta^{18}O$ is the simulated Cretaceous $\delta^{18}O$ plus 1.0‰ (SMOW).

[b]Ocean bathymetry of K-Bathy experiment is based on reconstructions from the PALEOMAP project (http://www.scotese.com/).

pleted with modern geography, ocean bathymetry and atmospheric pCO_2. The modern experiments differ only in their resolution of the Bering Strait. On the T31 grid, the Bering Strait is too narrow to be fully resolved. As a result, in the first experiment (MOD), the Bering Strait is not represented; that is, there is no ocean connection between the North Pacific and Arctic Oceans. To evaluate the influence of this ocean connection on high-latitude seawater $\delta^{18}O_w$, a second experiment (MOD-Bering) was conducted in which the bathymetry has been modified to include a Bering Strait connecting the North Pacific and Arctic Oceans. Though the model representation of the strait is narrow (3 grid cells in width), it nonetheless exaggerates the width of the modern strait.

[15] Two Cretaceous experiments were also completed with Cretaceous geography and topography representing Cenomanian lowstand conditions (as in the work by *Poulsen et al.* [2007b]). Middle Cretaceous atmospheric pCO_2 likely ranged between 2 and 14x preindustrial levels [*Bice et al.*, 2006]; in this study we used a median Cretaceous pCO_2 value of 2240 ppmv, 8x preindustrial levels. In the first Cretaceous experiment (K-Flat), the ocean bathymetry is uniformly 5600 m. In the second Cretaceous experiment (K-Bathy), we included Cretaceous paleobathymetry based on reconstructions from the PALEOMAP project (http://www.scotese.com/). Ocean $\delta^{18}O_w$ was initialized to 0.0‰ in the modern experiments and −1.0‰ (SMOW) in the Cretaceous experiments to reflect the absence of major ice sheets at that time [*Shackleton and Kennett*, 1975]. However, unless otherwise noted, we refer to and show "corrected" $\delta^{18}O$, which is the simulated Cretaceous $\delta^{18}O$ plus 1.0‰ (SMOW) to compensate for differences between modern and Cretaceous mean seawater $\delta^{18}O_w$, to facilitate comparison with the modern experiments. All analyses were made with the last 10 years of climate data from the final 35 year coupled iteration.

3. Results

3.1. Simulation of Modern $\delta^{18}O$

[16] GENESIS has previously been shown to simulate the large-scale modern surface $\delta^{18}O$ distribution including east-west gradients due to continental and altitudinal effects, seasonal variations, and the zonal profile except over Antarctica [*Mathieu et al.*, 2002]. Because our coupling of GENESIS 3.0 with MOM2 is a major revision, in this section we compare our simulated isotope composition of precipitation ($\delta^{18}O_p$) and surface seawater ($\delta^{18}O_w$) with modern observational data sets from *Rozanski et al.* [1993] and *LeGrande and Schmidt* [2006], which was based on the *Schmidt et al.* [1999] online database of $\delta^{18}O_w$ and salinity measurements.

[17] In the zonal mean, modeled precipitation $\delta^{18}O_p$ agrees well with IAEA/WMO data [*Rozanski et al.*, 1993] where data coverage is relatively dense. As shown in Figure 1, the 2σ uncertainty of zonally averaged $\delta^{18}O_p$ encloses nearly all the observed data. Since observational data is sparse or nonexistent in southern high latitudes, it is impossible to evaluate the model's performance in this region.

[18] The annual average surface seawater $\delta^{18}O_w$ captures most large-scale features in the *LeGrande and Schmidt* [2006] data set (compare Figures 2a and 2b). The model

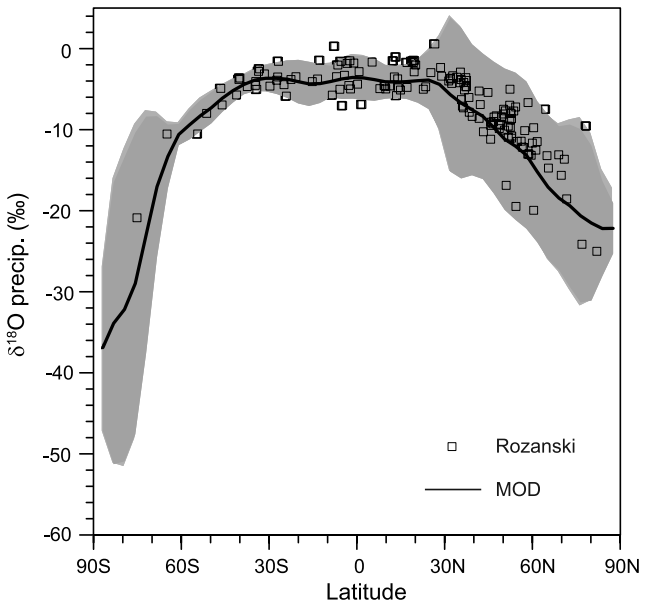

Figure 1. Mean annual zonal average $\delta^{18}O_p$ (SMOW) of precipitation predicted in our MOD experiment and from IAEA/WMO data [*Rozanski et al.*, 1993]. The shaded area is 2σ confidence interval of simulated zonally averaged $\delta^{18}O_p$.

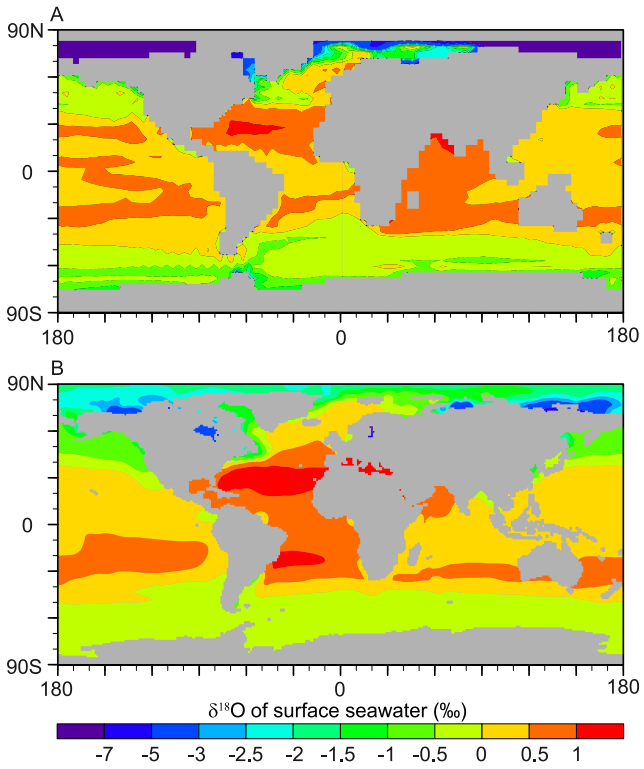

Figure 2. Mean annual $\delta^{18}O_w$ (SMOW) spatial distribution of modern surface seawater (a) predicted in our MOD experiment and (b) interpolated from global gridded empirical data [*LeGrande and Schmidt*, 2006]. Continental regions are shaded in gray.

predicts enriched surface seawater $\delta^{18}O_w$ in the subtropical oceans (especially in the Atlantic), and depleted surface seawater $\delta^{18}O_w$ in the Arctic and Southern Oceans. Surface seawater $\delta^{18}O_w$ differences between our MOD experiment and observation are generally within 0.5‰ except in the Arctic Ocean. In the zonal mean, the average surface seawater $\delta^{18}O_w$ in MOD experiment is within 2σ error range of the averaged $\delta^{18}O_w$ from *LeGrande and Schmidt* [2006] at low and middle latitudes (Figure 3a). At high latitudes, simulated $\delta^{18}O_w$ is depleted by up to 1‰ in the Southern Ocean and 11‰ in the Arctic Ocean. These large differences in the Arctic are due to the absence of a Bering Strait and connections between western and eastern Arctic Ocean. Without these gateways, no mixing occurs between the Arctic and Pacific Oceans. Consequently, Arctic $\delta^{18}O_w$ is driven to low values approaching those of the high-latitude continental runoff. In the MOD-Bering experiment, in which the Bering Strait has been opened and widened, the $\delta^{18}O_w$ difference between the model and observations in the Arctic is less than 2‰ (Figure 3a). In the Southern Ocean, the observed surface seawater $\delta^{18}O_w$ is derived from empirical $\delta^{18}O$-salinity relationships. The coefficient of determination (R^2) between $\delta^{18}O_w$ and salinity is 0.374, suggesting the Southern Ocean surface seawater $\delta^{18}O_w$ is not well characterized [*LeGrande and Schmidt*, 2006]. At this point, it is impossible to determine whether model

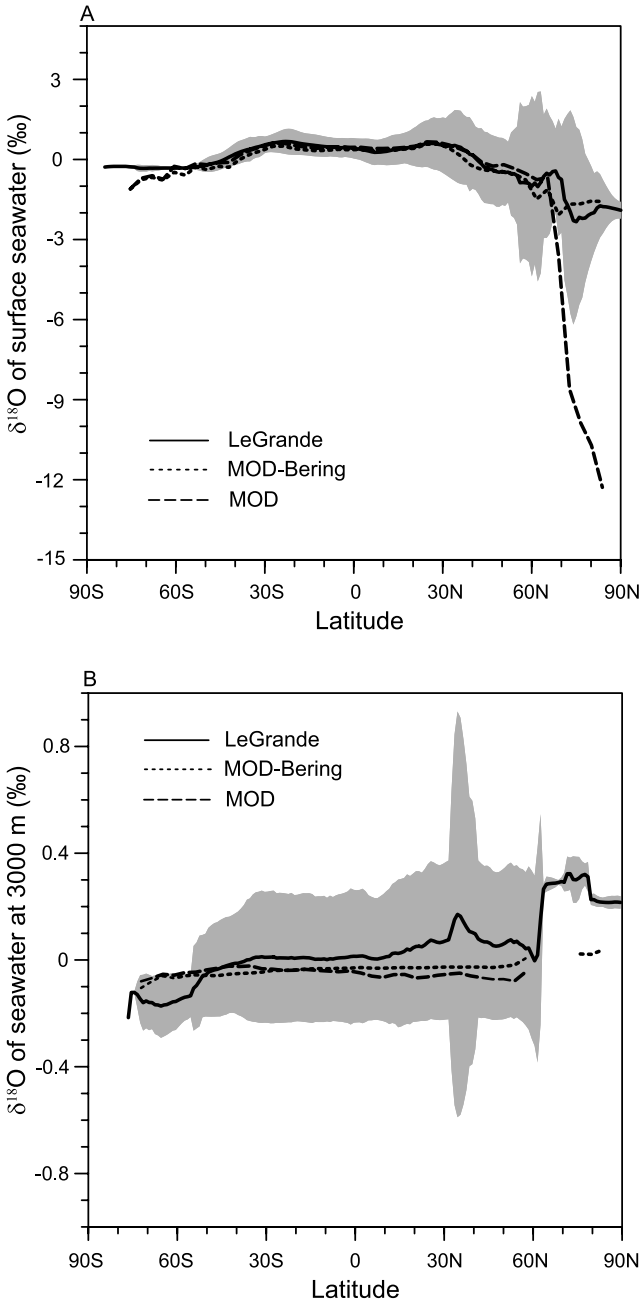

Figure 3. Mean annual zonal average $\delta^{18}O_w$ (SMOW) of (a) modern surface seawater and (b) modern deep water at 3000 m predicted in our MOD (medium dashed line) and MOD-Bering (short dashed line) experiments and from *LeGrande and Schmidt* [2006] (solid line). The shaded area is the 2σ confidence interval of zonally averaged $\delta^{18}O_w$ from *LeGrande and Schmidt* [2006] and represents spatial variability due to zonal heterogeneity in $\delta^{18}O_w$. Note that the MOD experiment has Arctic seawater $\delta^{18}O_w$ of -12‰ (see discussion in text). This low value is outside of the range shown in the figure.

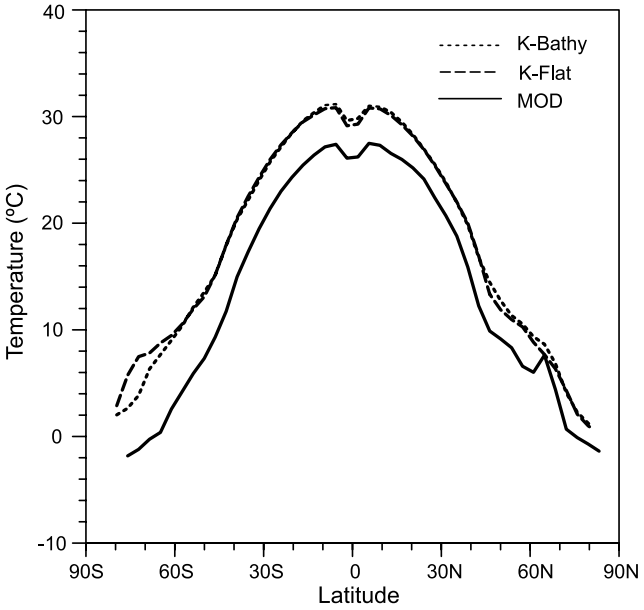

Figure 4. Mean annual zonal average sea-surface temperature in MOD (solid line), K-Flat (medium dashed line), and K-Bathy (short dashed line) experiments.

errors or observational uncertainties are chiefly responsible for the 1‰ discrepancy.

[19] The simulation of deep water $\delta^{18}O_w$ also compares well with observations. Seawater $\delta^{18}O_w$ at 3000 m is within 2σ of the *LeGrande and Schmidt* [2006] $\delta^{18}O_w$ except in the Arctic (Figure 3b). As described above, the differences in the Arctic region are attributed to insufficient mixing between the Arctic Ocean and Atlantic and Pacific Oceans. In sum, GENESIS-MOM reproduces modern observed seawater $\delta^{18}O_w$ in most regions where a meaningful comparison is possible.

3.2. Simulation of Cretaceous Climate and Precipitation $\delta^{18}O$

[20] As a result of higher CO_2 in our Cretaceous experiments, simulated surface temperature and precipitation rate are higher than present, consistent with previous Cretaceous simulations [e.g., *Barron et al.*, 1989; *Donnadieu et al.*, 2006; *Poulsen et al.*, 1999a, 2003, 2007b]. The global mean annual Cretaceous sea-surface temperature is 23.0°C, approximately 4.6°C higher than that in the MOD simulation (Table 1 and Figure 4). The global precipitation rate is 3.5 mm/d,$^{-1}$ about 0.5 mm/d higher than those simulated in the MOD experiment (Table 1).

[21] Cretaceous precipitation $\delta^{18}O_p$ ranges from −3.5‰ in subtropical areas to −20.8‰ (K-Flat) and −20.4‰ (K-Bathy) in the Antarctica regions (Figure 5). Cretaceous $\delta^{18}O_p$ in tropical and subtropical areas is practically identical to MOD. However, Cretaceous $\delta^{18}O_p$ is up to 16‰ and 5‰ greater than MOD in the southern high latitudes and Arctic region, respectively. Several factors are responsible for the enrichment of Cretaceous high-latitude precipitation including (1) reduced equilibrium fractionation due to higher polar temperatures, (2) reduced altitudinal fractionation in the Southern Hemisphere due to the absence of a tall Antarctic ice sheet, and (to a smaller degree) (3) a source of relatively high $\delta^{18}O$ vapor from a seasonally ice-free Arctic Ocean.

[22] Precipitation $\delta^{18}O_p$ is indistinguishable between the K-Flat and K-Bathy experiments except at northern high latitudes where the difference is ~1.4‰ (Figure 5). Because surface temperature and precipitation rate are nearly identical in these experiments, northern high-latitude precipitation $\delta^{18}O_p$ differences are likely due to differences in the isotopic concentration of the Arctic Ocean, which is seasonally ice-free and serves as an important regional vapor source. In the K-Flat experiment, Arctic seawater $\delta^{18}O_w$ is 4.4‰ greater than in the K-Bathy experiment because of enhanced seawater exchange between the Pacific and Arctic basins (see below), leading to greater precipitation $\delta^{18}O_p$.

3.3. Simulation of Cretaceous Surface Seawater $\delta^{18}O_w$

[23] The large-scale surface seawater $\delta^{18}O_w$ in the Cretaceous experiments is similar to the modern simulation. As in the MOD experiment, Cretaceous $\delta^{18}O_w$ is depleted in high latitudes and enriched in the subtropical oceans (Figures 6a and 6b). In the zonal mean, the Cretaceous surface seawater $\delta^{18}O_w$ distribution pattern is similar to modern in most areas, ranging from 0.3‰ in the subtropical oceans to −4.2‰ (K-Flat) and −8.6‰ (K-Bathy) in the Arctic (Figure 7). Cretaceous surface seawater $\delta^{18}O_w$ is ~0.3‰ lighter than modern in tropical and subtropical regions. The $\delta^{18}O_w$ difference is even smaller at the southern middle to

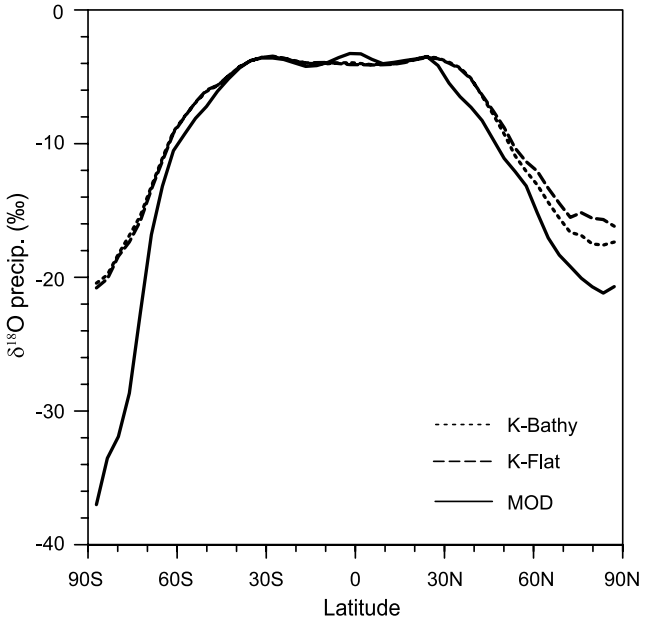

Figure 5. Mean annual zonal average precipitation $\delta^{18}O_p$ (SMOW) in MOD (solid line), K-Flat (medium dashed line), and K-Bathy (short dashed line) experiments. Note that "corrected" Cretaceous $\delta^{18}O$ is shown. As described in section 2, 1.0‰ (SMOW) has been added to the simulated Cretaceous $\delta^{18}O$ to facilitate comparison with the modern simulation.

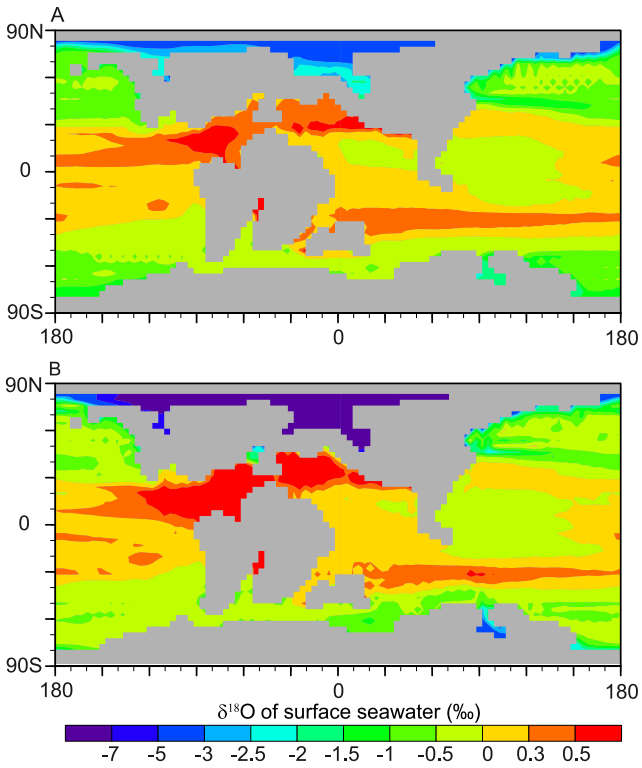

Figure 6. Mean annual $\delta^{18}O_w$ (SMOW) spatial distribution of Cretaceous surface seawater predicted for the (a) K-Flat experiment and (b) K-Bathy experiment. Continental regions are shaded in gray. Note that "corrected" Cretaceous $\delta^{18}O$ is shown (see caption in Figure 5).

high latitudes, which is ~0.1‰. In the Arctic Ocean, however, Cretaceous $\delta^{18}O_w$ is up to 8.1‰ (K-Flat) and 4.2‰ (K-Bathy) greater than that in the MOD experiment, but as much as 2.6‰ (K-Flat) and 7.0‰ (K-Bathy) lower than that in the MOD-Bering experiment. As discussed in 3.1, these differences between Cretaceous and modern Arctic $\delta^{18}O_w$ are due primarily to ocean mixing rates between the Arctic and Pacific Oceans. Similarly, differences in Arctic $\delta^{18}O_w$ between the Cretaceous simulations are also attributed to differences in Arctic-Pacific mixing rates. In the K-Flat experiment, with a deep (5600 m) paleo-Bering Strait and greater seawater exchange between the Pacific and Arctic, Arctic Ocean $\delta^{18}O_w$ is 4.4‰ higher than in the K-Bathy experiment with a shallow (144 m) strait and reduced seawater exchange.

3.4. Simulation of Cretaceous Subsurface Seawater $\delta^{18}O_w$

[24] In the most general sense, simulated Cretaceous subsurface seawater $\delta^{18}O_w$ is similar to modern. In both modern and Cretaceous experiments, the upper ocean (~150–1000 m) is more enriched in ^{18}O than the lower ocean (>1000 m), reflecting the preference for intermediate and deep water formation at high-latitude sites with relatively low $\delta^{18}O_w$. Moreover, at depths greater than 500 m, mean Cretaceous subsurface $\delta^{18}O_w$ is within 0.1‰ of modern (Figure 8).

[25] Though generally similar, there are meaningful differences between the modern and Cretaceous subsurface $\delta^{18}O_w$. In comparison to the modern, Cretaceous subsurface $\delta^{18}O_w$ is lower in the upper ocean and higher in the deep ocean (Figure 8). These differences result from the sites of intermediate and deep water formation. In both Cretaceous experiments, subtropical waters from the Tethys and proto–South Atlantic regions contribute significantly to the overall intermediate and deep water volumes. In the upper ocean (Figure 9a), saline, ^{18}O-enriched seawater originates from the Tethys and flows through the equatorial Pacific Ocean. This water mass is constrained to ~1400 m. At greater depths (Figure 9b), the North Pacific region provides the primary source of ^{18}O-enriched seawater. However, because North Pacific surface $\delta^{18}O_w$ is relatively depleted (Figure 6a), it cannot be the sole source of this water. Rather, warm, saline, ^{18}O-enriched seawater from Tethys flows into the North Pacific, mixes with colder North Pacific water, and sinks to form this water mass. Finally, at the greatest depths (Figure 9c), the proto–South Atlantic is a significant source of saline, ^{18}O-enriched seawater. Above, we have focused on the sources of relatively ^{18}O-enriched seawater. However, in both Cretaceous experiments, high-latitude regions around Antarctica are also important sites of intermediate and deep water formation (Figures 9b and 9c).

4. Discussion

4.1. Simulation of Cretaceous Surface Seawater $\delta^{18}O_w$

[26] To our knowledge, this study is the first to simulate Cretaceous seawater $\delta^{18}O_w$ using a coupled atmosphere-

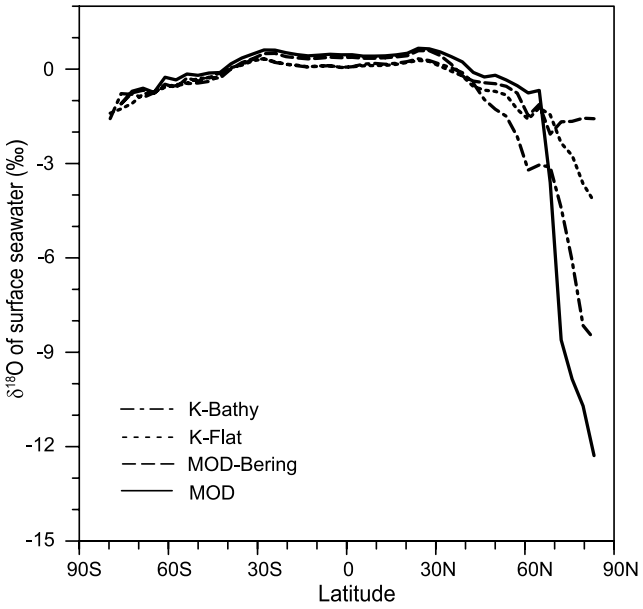

Figure 7. Mean annual zonal average $\delta^{18}O_w$ (SMOW) of surface seawater in MOD (solid line), MOD-Bering (medium dashed line), K-Flat (short dashed line), and K-Bathy (dash-dotted line) experiments. Note that "corrected" Cretaceous $\delta^{18}O$ is shown (see caption in Figure 5).

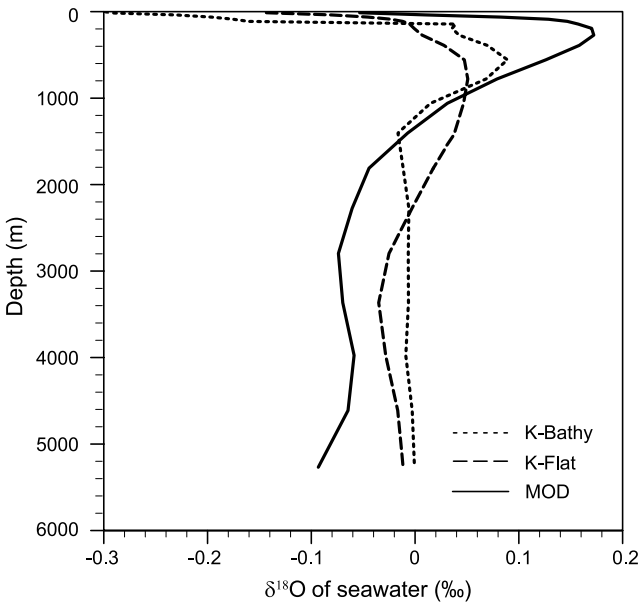

Figure 8. Vertical distribution of global mean seawater $\delta^{18}O_w$ (SMOW) in the modern and Cretaceous simulations. Cretaceous $\delta^{18}O_w$ is less above ~1000 m and greater below ~1000 m than modern because of differences in the isotopic composition of intermediate and deep water sources. Note that "corrected" Cretaceous $\delta^{18}O$ is shown (see caption in Figure 5).

ocean GCM with isotopic capabilities. *Poulsen et al.* [2007b] used an atmosphere-only model to demonstrate that high atmospheric pCO_2 causes a systematic, moderate (<3‰) increase in Cretaceous precipitation $\delta^{18}O_p$ resulting from reduced equilibrium fractionation due to higher surface temperatures. Although precipitation $\delta^{18}O_p$ can be strongly influenced locally by geography and topography, the large-scale $\delta^{18}O_p$ distribution changes little because it is controlled by the large-scale atmospheric circulation [*Poulsen et al.*, 2007b].

[27] Our results build on this previous study, and indicate that global ocean circulation has a small but important influence on the large-scale distribution of Cretaceous seawater $\delta^{18}O_w$. (The exception occurs in isolated basins, such as the Arctic Ocean and proto–South Atlantic Ocean, where the local precipitation flux can have a large influence on $\delta^{18}O_w$.) In our simulations, Cretaceous surface seawater $\delta^{18}O_w$ is ~0.3‰ less than modern at the low and middle latitudes. This decrease in surface seawater $\delta^{18}O_w$ is mainly due to differences in the partitioning of ^{18}O between the surface and the deep ocean. In the modern ocean, intermediate and deep water is formed primarily in high-latitude oceans, regions with relatively depleted surface $\delta^{18}O_w$ [*Frew et al.*, 1995]. In the Cretaceous experiments, the subtropical Tethys and proto–South Atlantic Oceans, regions with relatively high surface seawater $\delta^{18}O_w$, are important sources of intermediate and deep waters. The transport of these waters from the surface to depth lowers surface $\delta^{18}O_w$ and increases subsurface $\delta^{18}O_w$. This process of ^{18}O segregation in the ocean is the "compensation effect" described by *Roche et al.* [2006].

[28] *Roche et al.* [2006] report on changes in seawater $\delta^{18}O_w$ under warm climate conditions using CLIMBER-2, a coupled ocean-atmosphere model of intermediate complexity, and reach different conclusions from those presented here. Their model results predict an increase in low- and

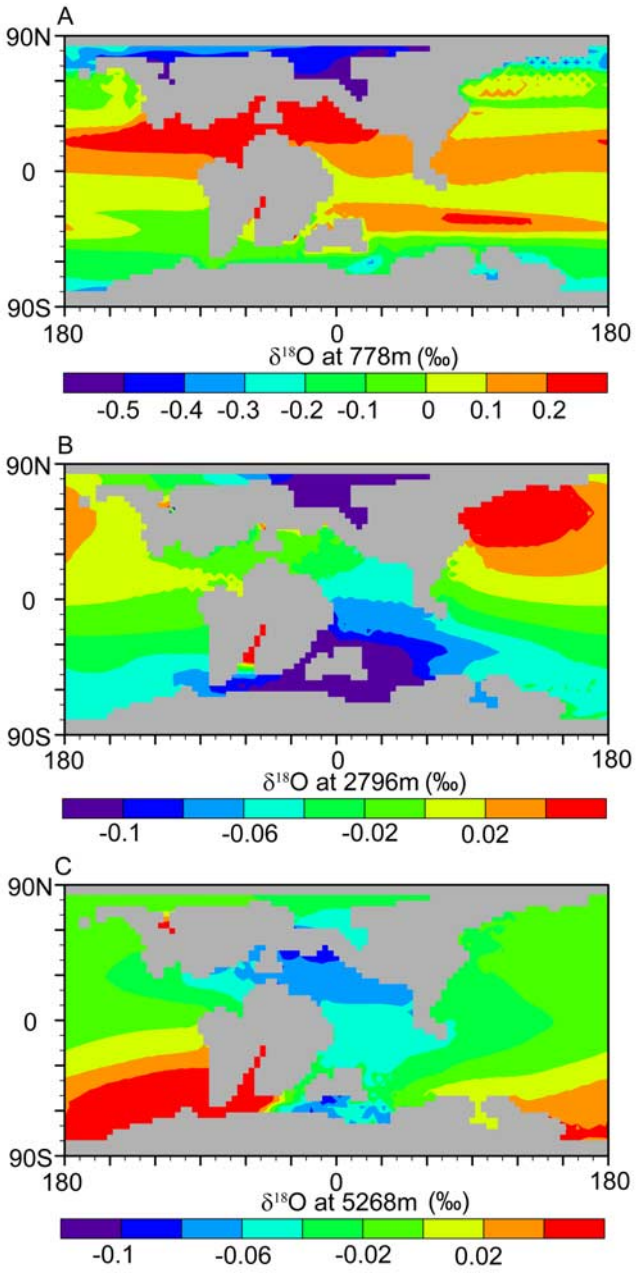

Figure 9. Mean annual $\delta^{18}O_w$ (SMOW) spatial distribution of Cretaceous seawater in K-Flat experiment (a) at depth of 778 m, (b) at depth of 2796 m, and (c) at depth of 5268 m. Continental regions are shaded in gray. The mean annual $\delta^{18}O_w$ distribution for the K-Bathy experiment is similar. Note that "corrected" Cretaceous $\delta^{18}O$ is shown (see caption in Figure 5).

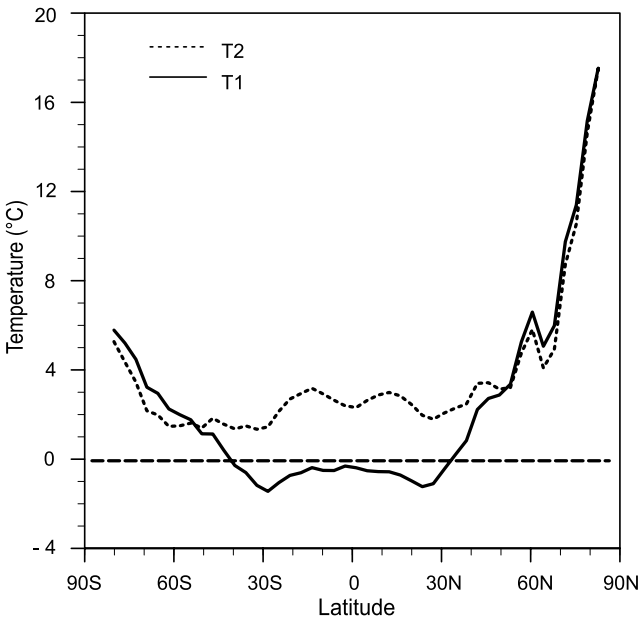

Figure 10. Comparison of temperature estimates using different assumptions about Cretaceous seawater $\delta^{18}O_w$. T1 ($T_{uniform} - T_{K\text{-}Flat}$) (solid line) denotes the temperature difference that results from assuming a uniform global mean surface seawater $\delta^{18}O_w$ of −1.0‰ (SMOW) rather than the $\delta^{18}O_w$ predicted in K-Flat. T2 ($T_{present} - T_{K\text{-}Flat}$) (dashed line) denotes the temperature difference that results from using present latitudinal $\delta^{18}O_w$ distribution from *Zachos et al.* [1994] rather than the $\delta^{18}O_w$ from K-Flat. As discussed in the text, we here use the "uncorrected" Cretaceous $\delta^{18}O_w$ from our simulation and the *Zachos et al.* [1994] $\delta^{18}O_w$ minus 1.0‰ (SMOW).

middle-latitude surface $\delta^{18}O_w$ by up to 1‰. There are two major differences between our studies. First, *Roche et al.* [2006] use a modern geography. In contrast to the modern, the Cretaceous geography includes subtropical basins that are not well connected to the global ocean and consequently evolved distinct water mass properties [*Poulsen et al.*, 2001] including relatively enriched $\delta^{18}O_w$. Second, in the work by *Roche et al.* [2006], water vapor isotopes are not tracked explicitly but are based on "simpler physical hypotheses. "Using this methodology, *Roche et al.* [2006] report increased transport of $\delta^{18}O$-depleted humidity to high latitudes in a warmer world, leading to a decrease in high-latitude $\delta^{18}O_w$. High-latitude deepwater formation and the "compensation effect" then cause the deep ocean to become relatively depleted in ^{18}O and the surface ocean to become enriched. In contrast, with water isotope tracer capabilities, GENESIS predicts $\delta^{18}O$-enriched vapor and precipitation at high latitudes as a result of a reduction in equilibrium fractionation in a warmer (high CO_2) world [*Poulsen et al.*, 2007b].

4.2. Implications for Oxygen Isotope Paleothermometry

[29] Oxygen isotope paleothermometry, arguably the most valuable tool in reconstructing past climate, requires knowledge of past seawater $\delta^{18}O_w$. In the absence of this information, previous studies have assumed that past seawater $\delta^{18}O_w$ was constant or the same as modern. Our simulation of Cretaceous $\delta^{18}O_w$ allows us to assess these assumptions, and their influence on paleotemperature estimates. Here, we calculate and compare paleotemperature estimates using constant (−1.0‰ SMOW), present-day, and simulated seawater $\delta^{18}O_w$. The present-day $\delta^{18}O_w$ distribution is based on a best fit to surface seawater $\delta^{18}O_w$ from Southern Hemisphere Atlantic and Pacific Oceans and describes $\delta^{18}O_w$ distribution the as a function of latitude [*Zachos et al.*, 1994]. In comparison to the *LeGrande and Schmidt* [2006] data, the *Zachos et al.* [1994] present-day $\delta^{18}O_w$ distribution is systematically higher, ranging from an increase of 0.02‰ at ~30°N to as much as 2.2‰ in the Arctic region, and no more than 0.3‰ in the Southern Hemisphere.

[30] Following *Roche et al.* [2006], we use the temperature-$\delta^{18}O$ equation from *Shackleton* [1974]:

$$T = 16.9 - 4.38(\delta^{18}O_c - \delta^{18}O_w) + 0.1(\delta^{18}O_c - \delta^{18}O_w)^2 \quad (1)$$

where $\delta^{18}O_c$ and $\delta^{18}O_w$ denote the oxygen isotopic content of foraminiferal calcite and seawater, respectively. To estimate the temperature bias (ΔT) due to the various assumptions about $\delta^{18}O_w$ (Δ ($\delta^{18}O_w$)), we derive the first-order Taylor expansion of (1), which is:

$$\Delta T \sim 4.18\Delta(\delta^{18}O_w) \quad (2)$$

Expression (2) indicates that $\delta^{18}O_w$ is a significant factor in calculating paleotemperature. Similar results would be derived using other temperature-$\delta^{18}O_w$ relationships [*Bemis et al.*, 1998, Table 1].

[31] We use (2) to compare the influences of common $\delta^{18}O_w$ assumptions and our simulated $\delta^{18}O_w$ on paleotemperature estimates. (Note that here we use "uncorrected" Cretaceous $\delta^{18}O_w$ from our simulation, and the values from *Zachos et al.* [1994] minus 1.0‰ to account for the absence of Cretaceous polar ice sheets.) In comparison to paleotemperatures estimated using our simulated zonal average Cretaceous $\delta^{18}O_w$, paleotemperatures estimated using either a uniform $\delta^{18}O_w$ (−1.0‰) or the *Zachos et al.* [1994] present-day distribution of $\delta^{18}O_w$ generally overestimate paleotemperatures (Figure 10). At high latitudes, this temperature overestimate is substantial, ranging from 2 to 17.6°C. Using the *Zachos et al.* [1994] present-day $\delta^{18}O_w$ also leads to substantially higher (~3°C) paleotemperature at low latitudes.

[32] The use of zonal average $\delta^{18}O_w$ is another important source of uncertainty in calculating paleotemperature. Our model results indicate that local $\delta^{18}O_w$ can vary by more than 1.5‰ from zonal average $\delta^{18}O_w$ at high latitudes (Figure 11), leading to isotopic paleotemperatures that differ up to 6°C according to (2). These large zonal differences in $\delta^{18}O_w$ occur in latitudinal zones with isolated or semi-isolated basins, including the Arctic, northern Tethys, and northern South Atlantic oceans. In these regions where

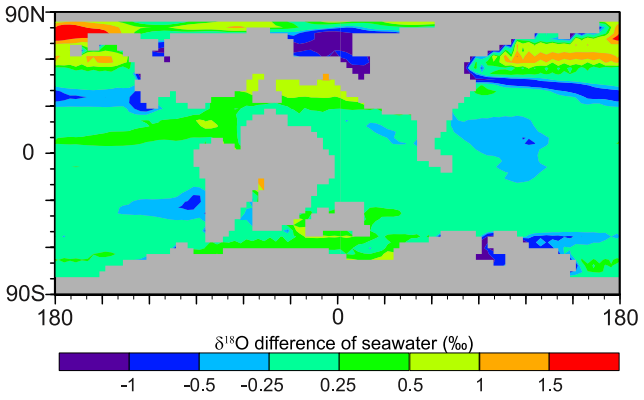

Figure 11. Mean annual $\delta^{18}O_w$ (SMOW) difference between local and zonal average surface seawater. For each grid cell, the $\delta^{18}O_w$ difference is obtained by subtracting the zonal average $\delta^{18}O_w$ at that latitude from the local $\delta^{18}O_w$.

seawater exchange is limited by features of the paleogeography, the surface $\delta^{18}O_w$ is more strongly influenced by local precipitation $\delta^{18}O_p$ and deviates from open ocean $\delta^{18}O_w$.

[33] The simulation of the Cretaceous equator-to-pole temperature gradient has been a long-standing problem [*Barron*, 1983; *Poulsen et al.*, 1999b; *Poulsen*, 2004; *Bice et al.*, 2003]. Proxy data, most notably $\delta^{18}O$ paleothermometry, has been used to infer that the equator-to-pole temperature gradient was small mainly as a result of very warm high-latitude paleotemperatures [e.g., *Huber et al.*, 1995]. In contrast, climate models have traditionally simulated large Cretaceous equator-to-pole temperature gradients. This mismatch has typically been attributed to flaws in the climate models stemming from, for example, the treatment of heat transport and clouds [e.g., *Barron*, 1994; *Sloan and Pollard*, 1998; *Kump and Pollard*, 2008]. Here, we emphasize another source of potential model-data mismatch, the interpretation of proxy data. Our calculation of Cretaceous seawater $\delta^{18}O_w$ substantially ameliorates the model-data mismatch by reducing the temperature inferred from high-latitude calcite $\delta^{18}O_c$. We do not claim to have solved this problem; other types of nonisotopic proxy data also suggest that the Cretaceous high-latitude temperatures were warm, and site specific model-data intercomparisons are still required to fully assess the significance of the $\delta^{18}O_w$ effect on isotopic paleotemperatures. However, we do view this as an important step forward, one that is critical to truly assessing the capability of models to simulate past warm worlds.

4.3. Oceanic Gateways, Continental Runoff, and Seawater $\delta^{18}O_w$

[34] Our modern and Cretaceous experiments indicate that the resolution of oceanic gateways can substantially influence regional seawater $\delta^{18}O_w$ (Figure 7). In both modern and Cretaceous experiments, the Bering Strait is critical to ocean mixing and isotopic exchange between the Pacific and Arctic Oceans. With no or weak exchange, Arctic seawater $\delta^{18}O_w$ will tend to resemble the high-latitude precipitation that feeds it. The implications of these results are twofold. First, paleogeography can be a first-order control on regional seawater $\delta^{18}O_w$. Second, in the absence of detailed knowledge about paleogeographic evolution, oxygen isotopic records should be interpreted with caution. Paleogeographic or eustatic changes that alter regional circulation and seawater $\delta^{18}O_w$ could be misconstrued as climatic change. Isotopic proxies from semi-isolated ocean basins would be particularly susceptible to this influence. Similar caveats on the interpretation of marine water isotope records have been found in other isotopic GCM experiments for the Holocene [*Schmidt et al.*, 2007].

[35] Continental runoff is also potentially an important influence on seawater $\delta^{18}O_w$. In this study, we have uniformly distributed continental runoff over the surface of the ocean, and have not tracked runoff from specific drainage basins into the ocean. This treatment of runoff could influence the simulated isotopic content of seawater especially in semi-isolated basins. A river routing scheme, in which runoff from specified drainage basins flows into the ocean at a point source, is likely to enhance regional isotopic differences in many basins. For example, the seawater $\delta^{18}O_w$ of the Cretaceous Arctic Ocean, which is relatively depleted in ^{18}O because of net precipitation, is likely to become further reduced with inflow of high-latitude continental runoff. In addition to this direct effect on seawater $\delta^{18}O_w$, continental runoff could also alter the distribution of ^{18}O between the surface and deep ocean through its influence on deep water formation. *Bice et al.* [1997] have shown that the specification of continental runoff in an ocean general circulation model can substantially change the location of deep water formation.

5. Conclusions

[36] We have developed a coupled ocean-atmosphere general circulation model that successfully simulates many aspects of modern precipitation and seawater $\delta^{18}O$ distribution. When applied to the Cretaceous, the model predicts surface seawater $\delta^{18}O_w$ that is similar in many respects to modern. Differences from the modern include (1) a small decrease in low- and middle-latitude surface seawater $\delta^{18}O_w$ due to a decrease in equilibrium fractionation, and a "compensation effect" caused by partitioning of the heavy isotope in the deep ocean due to intermediate and deep water formation in subtropical basins, and (2) large changes in Arctic surface seawater $\delta^{18}O_w$ that are linked to differences in seawater exchange rates between the Pacific and Arctic Oceans. The similarity between modern and Cretaceous zonal average surface seawater $\delta^{18}O_w$ highlights the fact that surface $\delta^{18}O_w$ is mainly constrained by large-scale atmospheric and oceanic circulation patterns, which change little between the modern and Cretaceous except in regions where paleogeography creates isolated or semi-isolated ocean basins.

[37] Our results have important implications for oxygen isotope paleothermometry, and indicate that conventionally used assumptions of surface seawater $\delta^{18}O_w$ likely overestimate Cretaceous middle- and high-latitude temperature.

Compensating for these isotopic effects by using simulated $\delta^{18}O_w$ reduces the Cretaceous low equator-to-pole thermal gradient problem.

[38] **Acknowledgments.** This study was supported by grants (0433440 and 0310032) from the National Science Foundation's Atmospheric Program to C. Poulsen, D. Pollard, and T. White. We gratefully acknowledge constructive reviews by two anonymous reviewers and Editor E. Rohling.

References

Barron, E. J. (1983), A warm, equable Cretaceous: The nature of the problem, *Earth Sci. Rev.*, *19*, 305–338.

Barron, E. J. (1994), Chill over the Cretaceous, *Nature*, *370*, 415, doi:10.1038/370415a0.

Barron, E. J., W. W. Hay, and S. Thompson (1989), The hydrologic cycle: A major variable during Earth history, *Palaeogeogr. Palaeoclimatol. Palaeoecol.*, *75*, 157–174, doi:10.1016/0031-0182(89)90175-2.

Bemis, B. E., H. J. Spero, J. Bijima, and D. W. Lea (1998), Reevaluation of the oxygen isotopic composition of planktonic foraminifera: Experimental results and revised paleotemperature equations, *Paleoceanography*, *13*, 150–160, doi:10.1029/98PA00070.

Bice, K. L., E. J. Barron, and W. H. Peterson (1997), Continental runoff and early Cenozoic bottom-water sources, *Geology*, *25*, 951–954, doi:10.1130/0091-7613(1997)025<0951:CRAECB>2.3.CO;2.

Bice, K. L., B. T. Huber, and R. D. Norris (2003), Extreme polar warmth during the Cretaceous greenhouse? Paradox of the late Turonian $\delta^{18}O$ record at Deep Sea Drilling Project Site 511, *Paleoceanography*, *18*(2), 1031, doi:10.1029/2002PA000848.

Bice, K. L., D. Birgel, P. A. Meyers, K. A. Dahl, K. Hinrichs, and R. D. Norris (2006), A multiple proxy and model study of Cretaceous upper ocean temperatures and atmospheric CO_2 concentrations, *Paleoceanography*, *21*, PA2002, doi:10.1029/2005PA001203.

Donnadieu, Y., R. Pierrehumbert, R. Jacob, and F. Fluteau (2006), Modelling the primary control of paleogeography on Cretaceous climate, *Earth Planet. Sci. Lett.*, *248*, 426–437, doi:10.1016/j.epsl.2006.06.007.

Erez, J., and B. Luz (1983), Experimental paleotemperature equation for planktonic foraminifera, *Geochim. Cosmochim. Acta*, *47*, 1025–1031, doi:10.1016/0016-7037(83)90232-6.

Frew, R. D., K. J. Heywood, and P. F. Dennis (1995), Oxygen isotope study of water masses in the Princess Elizabeth Trough, Antarctica, *Mar. Chem.*, *49*, 141–153, doi:10.1016/0304-4203(95)00003-A.

Herman, A. B., and R. A. Spicer (1996), Palaeobotanical evidence for a warm Cretaceous Arctic Ocean, *Nature*, *380*, 330–333, doi:10.1038/380330a0.

Huber, B. T. (1998), Tropical paradise at the Cretaceous poles, *Science*, *282*, 2199–2200, doi:10.1126/science.282.5397.2199.

Huber, B. T., D. A. Hodell, and C. P. Hamilton (1995), Middle–Late Cretaceous climate of the southern high latitudes: Stable isotope evidence for minimal equator-to-pole thermal gradient, *Geol. Soc. Am. Bull.*, *107*, 1164–1191, doi:10.1130/0016-7606(1995)107<1164:MLCCOT>2.3.CO;2.

Jenkyns, H. C., A. Forster, S. Schouten, and J. S. S. Damsté (2004), High temperatures in the Late Cretaceous Arctic Ocean, *Nature*, *432*, 888–892, doi:10.1038/nature03143.

Joussaume, S., and J. Jouzel (1993), Paleoclimatic tracers: An investigation using an atmospheric general circulation model under ice age conditions: 2. Water isotopes, *J. Geophys. Res.*, *98*, 2807–2830, doi:10.1029/92JD01920.

Jouzel, J., D. Koster, R. J. Suozzo, and G. L. Russell (1994), Stable isotope behavior during the last glacial maximum. A general circulation model analysis, *J. Geophys. Res.*, *99*, 25791–25801, doi:10.1029/94JD01819.

Kiehl, J. T., J. J. Hack, G. B. Bonan, B. A. Boville, D. L. Williamson, and P. J. Rasch (1998), The National Center for Atmospheric Research Community Climate Model: CCM3, *J. Clim.*, *11*, 1131–1149, doi:10.1175/1520-0442(1998)011<1131:TNCFAR>2.0.CO;2.

Kim, S.-J., G. M. Flato, and G. J. Boer (2003), A coupled climate model simulation of the Last Glacial Maximum, part 2: Approach to equilibrium, *Clim. Dyn.*, *20*, 635–661.

Kolodny, Y., B. Luz, and O. Navon (1983), Oxygen isotope variations in phosphate of biogenic apatites. I. Fish bone apatite—Rechecking the rules of the game, *Earth Planet. Sci. Lett.*, *64*, 398–404, doi:10.1016/0012-821X(83)90100-0.

Kump, L. R., and D. Pollard (2008), Amplification of Cretaceous warmth by biological cloud feedbacks, *Science*, *320*, 195, doi:10.1126/science.1153883.

LeGrande, A. N., and G. A. Schmidt (2006), Global gridded data set of the oxygen isotopic composition in seawater, *Geophys. Res. Lett.*, *33*, L12604, doi:10.1029/2006GL026011.

Marotzke, J. (1991), Influence of convective adjustment on the stability of the thermohaline circulation, *J. Phys. Oceanogr.*, *21*, 903–907, doi:10.1175/1520-0485(1991)021<0903:IOCAOT>2.0.CO;2.

Mathieu, R. D., D. Pollard, J. E. Cole, J. W. C. White, R. S. Webb, and S. L. Thompson (2002), Simulation of stable water isotope variations by the GENESIS GCM for modern conditions, *J. Geophys. Res.*, *107*(D4), 4037, doi:10.1029/2001JD900255.

Moriya, K., P. A. Wilson, O. Friedrich, J. Erbacher, and H. Kawahata (2007), Testing for ice sheets during the mid-Cretaceous greenhouse using glassy foraminiferal calcite from the mid-Cenomanian tropics on Demerara Rise, *Geology*, *35, 615–618, doi:10.1130/G23589A.1.*

Nathorst, A. G. (1911), On the value of fossil floras of the Arctic regions as evidence of geological climate, *Geol. Mag.*, *8*, 217–225.

Norris, R. D., K. L. Bice, E. A. Magno, and P. A. Wilson (2002), Jiggling the tropical thermostat in the Cretaceous hothouse, *Geology*, *30*, 299–302, doi:10.1130/0091-7613(2002)030<0299:JTTTIT>2.0.CO;2.

Pacanowski, R. C. (1995), MOM2 documentation, user's guide and reference manual, version 1.0, *Tech. Rep. 3,* Ocean Group, Geophys. Fluid Dyn. Lab., NOAA, Princeton Univ., Princeton, N. J.

Parrish, J. T., and R. A. Spicer (1988), Late Cretaceous terrestrial vegetation: A near-polar temperature curve, *Geology*, *16*, 22–25, doi:10.1130/0091-7613(1988)016<0022:LCTVAN>2.3.CO;2.

Poulsen, C. J. (2004), A balmy Arctic, *Nature*, *432*, 814–815, doi:10.1038/432814a.

Poulsen, C. J., E. J. Barron, C. Johnson, and P. Fawcett (1999a), Links between major climatic factors and regional oceanic circulation in the mid-Cretaceous, in *Evolution of the Cretaceous Ocean-Climate System,* edited by E. Barrera, and C. C. Johnson, *Spec. Pap. Geol. Soc. Am., 332*, 73–90.

Poulsen, C. J., E. J. Barron, W. H. Peterson, and P. A. Wilson (1999b), A reinterpretation of mid- Cretaceous shallow marine temperatures through model-data comparison, *Paleoceanography*, *14*, 679–697, doi:10.1029/1999PA900034.

Poulsen, C. J., E. J. Barron, M. A. Arthur, and W. H. Peterson (2001), Response of the mid-Cretaceous ocean circulation to tectonic and CO_2 forcing, *Paleoceanography*, *16*, 576–592, doi:10.1029/2000PA000579.

Poulsen, C. J., A. S. Gendaszek, and R. L. Jacob (2003), Did the rifting of the Atlantic Ocean cause the Cretaceous thermal maximum?, *Geology*, *31*, 115–118, doi:10.1130/0091-7613(2003)031<0115:DTROTA>2.0.CO;2.

Poulsen, C. J., D. Pollard, I. S. Montanez, and D. Rowley (2007a), Late Paleozoic tropical climate response to Gondwanan deglaciation, *Geology*, *35*, 771–774, doi:10.1130/G23841A.1.

Poulsen, C. J., D. Pollard, and T. S. White (2007b), General circulation model simulation of the $\delta^{18}O$ content of continental precipitation in the middle Cretaceous: A model-proxy comparison, *Geology*, *35*, 199–202, doi:10.1130/G23343A.1.

Price, G. D. (1999), The evidence and implications of polar ice during the Mesozoic, *Earth Sci. Rev.*, *48*, 183–210, doi:10.1016/S0012-8252(99)00048-3.

Pucéat, E., C. Lécuyer, Y. Donnadieu, P. Naveau, H. Cappetta, G. Ramstein, B. T. Huber, and J. Kriwet (2007), Fish tooth $\delta^{18}O$ revising Late Cretaceous meridional upper ocean water temperature gradients, *Geology*, *35*, 107–110, doi:10.1130/G23103A.1.

Rahmstorf, S. (1993), A fast and complete convection scheme for ocean models, *Ocean Modell.*, *101*, 9–11.

Redi, M. H. (1982), Oceanic isopycnal mixing by coordinate rotation, *J. Phys. Oceanogr.*, *12*, 1154–1158, doi:10.1175/1520-0485(1982)012<1154:OIMBCR>2.0.CO;2.

Roche, D. M., Y. Donnadieu, E. Pucéat, and D. Paillard (2006), Effect of changes in $\delta^{18}O$ content of the surface ocean on estimated sea surface temperature in past warm climate, *Paleoceanography*, *21*, PA2023, doi:10.1029/2005PA001220.

Rozanski, K., L. Araguds-Araguds, and R. Gonfiantini (1993), Isotopic patterns in modem global precipitation, in Climate Change in *Continental Isotopic Records, Geophys. Monogr. Ser.*, vol. 78, edited by P. K. Swart, et al., pp. 1–36, AGU, Washington, D. C.

Schmidt, G. A., G. R. Bigg, and E. J. Rohling (1999), Global seawater oxygen-18 database,

http://data.giss.nasa.gov/o18data/, NASA Goddard Inst. for Space Stud., New York.

Schmidt, G. A., A. N. LeGrande, and G. Hoffmann (2007), Water isotope expressions of intrinsic and forced variability in a coupled ocean-atmosphere model, *J. Geophys. Res.*, *112*, D10103, doi:10.1029/2006JD007781.

Shackleton, N. (1974), Attainment of isotopic equilibrium between ocean water and the benthonic foraminifera genus Uvigerina: Isotopic changes in the ocean during the last glacial, in *Les méthodes quantitatives d'étude des variation du climat au cours du pléistocène*, edited by J. Labeyrie, pp. 203–209, Cent. Natl. de la Rech. Sci., Paris.

Shackleton, N., and J. Kennett (1975), Paleotemperature history of the Cenozoic and the initiation of Antarctic glaciation: Oxygen and carbon isotope analyses in DSDP Sites 277, 279 and 281, *Initial Rep. Deep Sea Drill. Proj.*, *29*, 743–755.

Sloan, L. C., and D. Pollard (1998), Polar stratospheric clouds: A high latitude warming mechanism in an ancient greenhouse world, *Geophys. Res. Lett.*, *25*, 3517–3520, doi:10.1029/98GL02492.

Spicer, R. A., and J. T. Parrish (1986), Paleobotanical evidence for cool north polar climates in middle Cretaceous (Albian-Cenomanian) time, *Geology*, *14*, 703–706, doi:10.1130/0091-7613(1986)14<703:PEFCNP>2.0.CO;2.

Tarduno, J. A., D. B. Brinkman, P. R. Renne, R. D. Cottrell, H. Scher, and P. Castillo (1998), Evidence for extreme climatic warmth from late Cretaceous Arctic vertebrates, *Science*, *282*, 2241–2244, doi:10.1126/science.282.5397.2241.

Thompson, S. L., and D. Pollard (1997), Greenland and Antarctic mass balances for present and doubled CO_2 from the GENESIS version-2 global climate model, *J. Clim.*, *10*, 871–900, doi:10.1175/1520-0442(1997)010<0871:GAAMBF>2.0.CO;2.

Voss, R., and R. Sausen (1996), Techniques for asynchronous and periodically synchronous coupling of atmosphere and ocean models, part II: Impact of variability, *Clim. Dyn.*, *12*, 605–614.

Wilson, P. A., R. D. Norris, and M. J. Cooper (2002), Testing the Cretaceous greenhouse hypothesis using glassy foraminiferal calcite from the core of the Turonian tropics on Demerara Rise, *Geology*, *30*, 607–610, doi:10.1130/0091-7613(2002)030<0607:TTCGHU>2.0.CO;2.

Zachos, J. C., L. D. Stott, and K. C. Lohmann (1994), Evolution of early Cenozoic marine temperatures, *Paleoceanography*, *9*, 353–387, doi:10.1029/93PA03266.

D. Pollard and T. S. White, Earth and Environment Science Institute, Pennsylvania State University, University Park, PA 16802, USA.

C. J. Poulsen and J. Zhou, Department of Geological Sciences, University of Michigan, Ann Arbor, MI 48109, USA. (zotsing@umich.edu)